Catalysis Science & Technology

Accepted Manuscript

ROYAL SOCIETY OF CHEMISTRY

www.rsc.org/catalysis

Catalysis Science & Technology RSC Publishing

PAPER

Low-temperature selective catalytic reduction of NOx with NH_3 over manganese and cerium oxides composite with graphene prepared by hydrothermal method

Received (in XXX, XXX) Xth XXXXXXXXX 20XX,

Accepted Xth XXXXXXXXX 20XX

DOI: 10.1039/b000000x

Xiang Xiao,[a,b] Zhongyi Sheng,[*,a,c] Liu Yang,[a,c] and Fan Dong[b,d]

[a] *Department of Environmental Science and Engineering, Nanjing Normal University, Nanjing 210023, China*

[b] *College of Environmental and Biological Engineering, Chongqing Technology and Business University, Chongqing, 400067, China*

[c] *Jiangsu Provincial Key Laboratory of Materials Cycling and Pollution Control, Nanjing 210023, China*

[d] *Chongqing Key Laboratory of Catalysis and Functional Organic Molecules, Chongqing, 400067, China*

MnOx-CeO_2/graphene (MnOx-CeO_2/GR) catalysts prepared by the hydrothermal method with different mass ratios of graphene (0-0.45 wt. %) were investigated for the low-temperature selective catalytic reduction (SCR) of NOx with NH_3. The as-prepared catalysts have been characterized systematically to elucidate their morphological structure and surface properties by XRD, SEM, TEM, BET, XPS, H_2-TPR, NH_3-TPD and FT-TR. It was found that the environmentally benign MnOx-CeO_2/GR (0.3% wt %) catalyst exhibited excellent NH_3-SCR activity and strong resistance against H_2O and SO_2, which is very competitive for the application in controlling the NOx emission from flue gas. On the basis of the catalyst characterization, high specific surface areas, the uniform distribution of active sites, as well as the interaction of manganese and cerium oxide species, played key roles in the excellent catalytic performance of MnOx-CeO_2/GR and resulted in improved SO_2 tolerance.

1. Introduction

Nitrogen oxides (NOx) emitted from the combustion of fossil fuels is one of the main atmospheric pollutants, which has given rise to a variety of health-related and environmental issues.[1-3] Low-temperature selective catalytic reduction (SCR) with NH_3 is a promising method to remove NOx in flue gas because the unit can be located downstream of the particulate control device and desulfurization system, where the temperature is about 120-180 °C.[4-6] Mn-containing catalysts exhibited relatively high activity for the low-temperature NH_3-SCR.[7-12] Besides, Ce-based NH_3-SCR catalysts have also been widely studied due to the high oxygen storage capacity and excellent redox property of CeO_2.[13-15] These works basically focused on improving the activity for low-temperature SCR catalyst. However, there is still certain amount of SO_2 in the exhausted gas, which could have a serious poisoning effect on SCR catalytic activity in the low temperature range.[16-18] Therefore, improving activity and SO_2 resistance of the low-temperature SCR catalysts have attracted wide concern.[19-22]

High specific surface areas can be provided by carbon materials, such as activated carbon (AC), activated carbon fiber (ACF), and carbon nanotubes (CNTs), which can also provide high chemical stability.[23-26] Among them, graphene (GR), a new carbon nanomaterial, which have large surface area (2600 m^2/g), flexible structure, and high chemical stability.[27-29] The high-efficiency process of the gain and loss of electrons has resulted in the improvement of the redox performance and the catalytic reduction ability of the catalyst. By introducing graphene into catalyst, loading of the active component (MnOx) was improved and adsorption of NH_3 was increased, hence the catalytic activity was enhanced. Therefore, graphene becomes a composite support achieving complementary advantages and the ability to improve the SCR performance. Lu et al. have focused on the application of graphene in the low-temperature SCR field.[30, 31]

So far, almost all the MnOx-CeO_2 catalysts studied were prepared by co-precipitation,[32] sol-gel,[33] and impregnation method.[34] As we know, the hydrothermal synthesis method has the advantages of simplicity, high efficiency, high purity and good homogeneity.[35] Liu et al.[16] have reported that Mn-Ce-Ti mixed-oxide catalyst prepared by the hydrothermal method exhibited excellent NH_3-SCR activity and strong resistance against H_2O and SO_2 with a broad operation temperature window.[16] In this work, a series of MnOx-CeO_2/GR catalysts were prepared by hydrothermal method, which few researchers have concerned about. To fully examine the structure and possible interaction between MnOx-CeO_2 and graphene, the catalysts were characterized by SEM, TEM, XRD, BET, H_2-TPR, NH_3-TPD, FT-IR and XPS.

2. Experimental section

2.1 Catalyst Preparation

The MnOx-CeO_2/GR catalysts with different mass ratios of GR were prepared by hydrothermal method. Appropriate amounts of $Mn(NO_3)2•3H_2O$, $Ce(NO_3)_3•6H_2O$, and graphene (XFNANO, dispersible graphene) were dissolved in deionized water at room

temperature and stirred for 20 min, then ammonia solution (28 wt%, 20 mL) was slowly added to the above solution under vigorous stirring until pH is ca. 11. After stirring for 30 min, the obtained suspension was transferred to a 250 ml Teflon-sealed autoclave and reacted at 130 °C for 12 h in an oven. The precipitate was separated by centrifuging and washed several times with distilled water and ethanol, respectively. The resulting powder was dried at 100 °C for 12 h and then calcined in air at 400 °C for 2 h. For comparison, MnOx/GR, CeO_2/GR, MnOx and CeO_2 catalysts were also prepared by the same preparation method as described above.

2.2 Catalyst Characterization

The morphology of the catalysts was characterized by scanning electron microscopy (SEM), transmission electron microscopy (TEM), and high-resolution TEM (HRTEM). The structure of the samples was determined by X-ray diffraction (XRD) obtained on a Bruker D8 Advance diffract meter. The surface areas of catalysts were calculated by Brunauer-Emmett-Teller (BET) method, with Micromeritics ASSP2020 equipment by N_2 physisorption at 77K. The surface atomic states of the catalysts were analyzed by X-ray photoelectron spectroscopy (XPS) with Thermo Escalab 250Xi. H_2 temperature-programmed reduction (H_2-TPR) and NH_3 temperature-programmed desorption (NH_3-TPD) were performed on a Tianjin XQ TP5080 auto-adsorption apparatus. Prior to H_2-TPR experiment, 50 mg of catalysts were pretreated with N_2 with a total flow rate of 30 mL·min^{-1} at 300°C for 0.5 h, then cooled down to room temperature in the N_2 atmosphere. Finally, the temperature was raised to 600°C with a constant heating rate of 10 °C·min^{-1} in a flow of H_2 (5 vol. %)/ N_2 (30 mL·min^{-1}). Prior to the NH_3-TPD experiments, the catalysts (150 mg) were pretreated at 300°C in a flow of N_2 (30 mL·min^{-1}) for 0.5 h and cooled to 100 °C under N_2 flow. Then the samples were exposed to a flow of NH_3 at 100 °C for 1 h, followed by N_2 purging for 0.5 h. Finally, the reactor temperature was raised to 800 °C in the N_2 flow at a constant rate of 10 °C·min^{-1}. The used catalyst was analyzed by Fourier transform infrared spectroscopy (FT-IR PROTÉGÉ 460, Thermo Nicolet) to reveal the poisoning effect of SO_2.

2.3 Catalytic Activity Tests

The SCR activity measurements were carried out in a fixed-bed reactor at 60-180 °C containing 4 mL catalyst with a gas hourly space velocity (GHSV) of 24,000 h^{-1}. The typical gas consisted of 500 ppm NO, 500 ppm NH_3, 0 or 200 ppm SO_2, 5% O_2, and balance N_2. NO, NO_2, SO_2, and O_2 were measured by a flue gas analyzer (MRU Vario Plus, Germany). NH_3 was analyzed with a portable NH_3 analyzer (Nantong Water Environmental Protection Technology Co.Ltd., Model MOT 400). NOx conversion and N_2 selectivity were calculated as follows: [9]

$$NO_x\ conversion(\%) = 100 \times \frac{C^{in}_{NO_x} - C^{out}_{NO_x}}{C^{in}_{NO_x}}$$

$$N_2\ selectivity(\%) = 100 \times \frac{C^{in}_{NO} + C^{in}_{NH_3} - C^{out}_{NO_2} - 2C_{N_2O}}{C^{in}_{NO} - C^{in}_{NH_3}}$$

3. Results and discussion

3.1 Morphology and texture

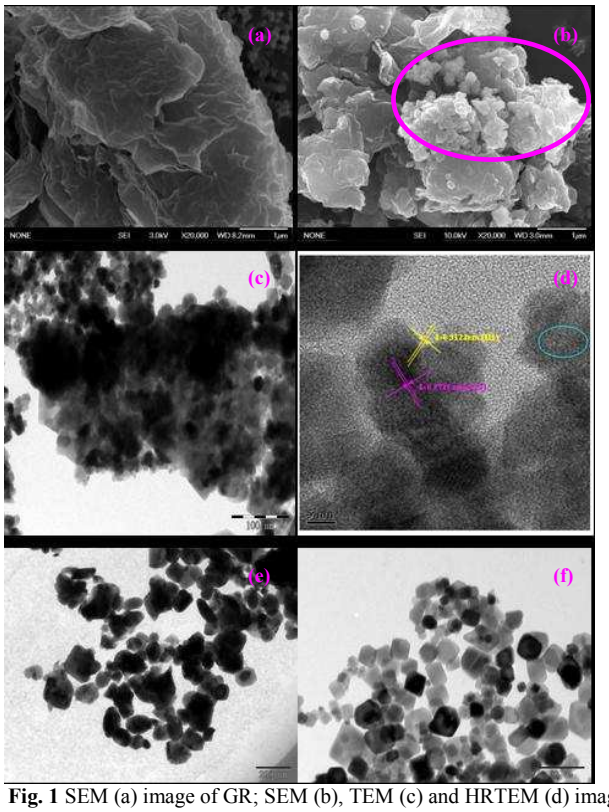

Fig. 1 SEM (a) image of GR; SEM (b), TEM (c) and HRTEM (d) images of MnOx-CeO_2/GR (0.3%); TEM (e) image of MnOx; TEM (f) image of CeO_2.

SEM image of graphene in Fig. 1a shows that GR is transparent with some clearly visible wrinkles, suggesting that graphene is mainly composed of single or few layers. From Fig. 1b, it is clear that a large number of MnOx-CeO_2 nanoparticles ranging from 5 to 25 nm, with average particle size of ca. 20 nm mounted on the stacked and wrinkled GR sheets. TEM image in Fig. 1c indicates that MnOx-CeO_2 nanoparticles are anchored onto the surface of GR sheet surfaces and some MnOx-CeO_2 particles are aggregated together. Fig. 1d shows the typical HRTEM image of MnOx-CeO_2/GR. The observed spacing between the lattice planes of the sample is 0.3123 nm and 0.2716 nm, corresponding to (111) crystallographic planes of CeO_2 and (222) crystallographic planes of Mn_2O_3, respectively. Fig. 1e shows a TEM image of MnOx, where the particles size of MnOx is estimated to be around 40-60 nm. Large MnOx nanoparticles are present within the prepared sample, indicating some particle aggregation. From Fig. 1f, it is clear that a large number of homogeneous CeO_2 nanocubes with average size of 20 nm are synthesis by the hydrothermal method.

3.2 XRD of the catalysts

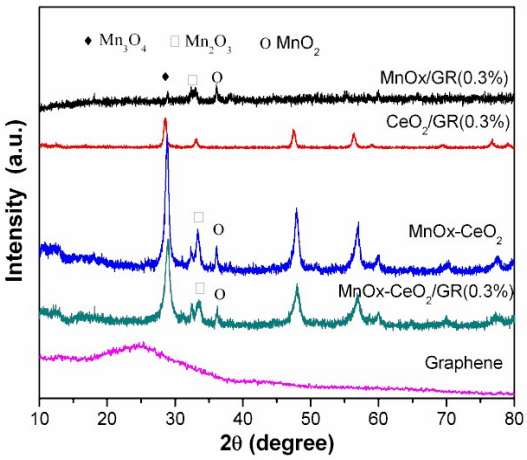

Fig. 2 XRD patterns of the catalysts

Fig. 2 shows the XRD patterns of the samples in the angular range 10°-80° 2θ. For MnOx/GR, the intensive and sharp diffractions at 32.9° could be primarily attributed to Mn_2O_3 (JCPDS 41-1442), the diffraction peaks for Mn_3O_4 were apparent in MnOx (JCPDS 65-2776), and meanwhile some weak diffraction peaks for MnO_2 (JCPDS 30-0820) were also visible. The diffraction peaks at 2θ = 28.5°, 33.0°, 47.4°, 56.4°, 59.2°, 70.4°, and 79.4° in the XRD profile of the CeO_2/GR clearly demonstrated the presence of cubic fluorite structure of CeO_2 (JCPDS 43-1002). For MnOx-CeO_2, the Mn_2O_3 and MnO_2 shifting slightly to the low value indicated that Mn^{3+} or Mn^{4+} species entered the lattice, leading to the formation of MnCeOx solid solution.[36] Owing to the redox property of Mn in the lattice, the solid solution was effective in promoting oxidative sorption of NO as nitrates.[37] No characteristic diffraction peaks for carbon species were observed in the MnOx-CeO_2/GR composite because of the low amount and relatively low diffraction intensity of graphene, while the existence of graphene was determined by the following XPS analysis. Furthermore, the peak intensities of MnOx-CeO_2/GR (0.3%) were lower than those of the MnOx-CeO_2, indicating that adding of GR resulted in the lower crystallinity of MnOx-CeO_2.

3.3 BET surface areas and pore size distributions

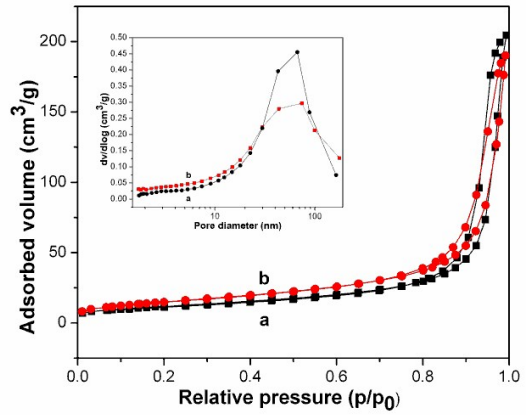

Fig. 3 Nitrogen adsorption-desorption isotherms and the corresponding size distribution curves (inset) of the catalysts: (a) MnOx-CeO_2 and (b) MnOx-CeO_2/GR (0.3%).

The specific surface area, pore volume, and pore size of the MnOx-CeO_2 and MnOx-CeO_2/GR (0.3%) are summarized in Table 1. MnOx-CeO_2/GR had the larger specific surface area, which leading to the high dispersion during the metal oxide composite with GR. The nitrogen adsorption-desorption isotherms and corresponding pore size distribution curves of the as-prepared samples are displayed in Fig. 3. According to the Brunauer-Deming-Deming-Teller (BDDT) classification, the majority of physisorption isotherms could be classified into six types. It could be clearly seen that the MnOx-CeO_2 and MnOx-CeO_2/GR (0.3%) could both be classified into the representative type IV adsorption-desorption isotherm with H_3-type hysteresis loop, revealing the mesoporous features, which could be resulted from the packing of nanoparticles. As illustrated in the inset of Fig. 3, the pore distribution of MnOx-CeO_2 and MnOx-CeO_2/GR show a pore size with an average pore size of 29.84 nm and 21.46 nm, respectively. Moreover, MnOx-CeO_2/GR (0.3%) present pore volume approximately equal to MnOx-CeO_2. These results indicated MnOx-CeO_2/GR (0.3%) had porous structures. The increased mesoporous were probably caused by the addition of GR that changed the dispersity of the metal oxide particles, consistent with the TEM observation (Fig. 1b). In general, the larger specific surface area and porous structures were expected to be useful in the catalytic performance by offering more active sites and adsorption of reactants, resulting in the latter excellent catalytic performance of MnOx-CeO_2/GR (0.3%).

Table 1 Porous Structure Parameters of MnOx-CeO_2 and MnOx-CeO_2/GR (0.3%) catalysts

Catalysts	BET surface area(m^2/g)	Pore volume ($\times10^{-2}cm^3$/g)	Average pore Diameter (nm)
MnOx-CeO_2	42.4322	31.6489	29.84
MnOx-CeO_2/GR(0.3%)	54.8432	30.8147	21.46

3.4. Chemical composition by XPS

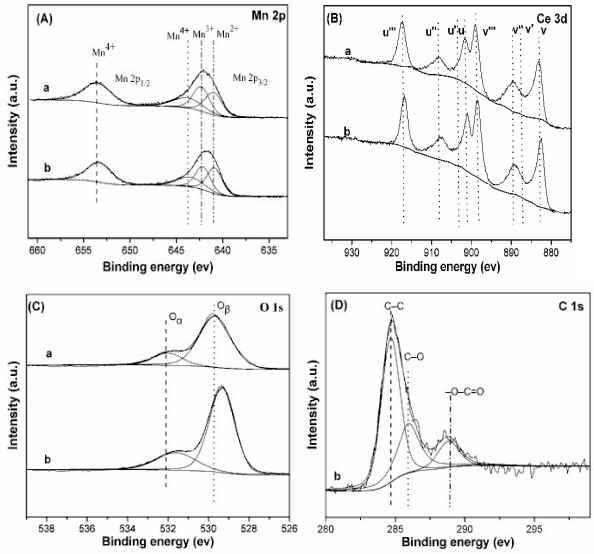

Fig. 4 XPS spectra for Mn 2p (A), Ce 3d (B), O 1s (C) and C1s (D) of the catalysts: (a) MnOx-CeO_2 and (b) MnOx-CeO_2/GR (0.3%).

Table 2 Atomic surface compositions of the MnOx-CeO_2, MnOx-CeO_2/GR (0.3%) obtained with XPS.

Samples	Atomic composition (%)											
	C	Mn	Ce	O	O		C			Mn		
					O_α	O_β	C-C	C-O	-O-C=O	MnO/ Mn	MnO_2/ Mn	Mn_2O_3/ Mn
MnOx-CeO_2	/	12.2	5.54	82.26	14.81	67.45	/	/	/	0.2652	0.4991	0.2357
MnOx-CeO_2/GR	0.025	9.953	6.344	83.453	20.363	63.09	0.01506	0.00616	0.00378	0.2356	0.5815	0.1829

The information on the atomic concentration and element chemical state on the catalysts surface was further investigated by XPS. Fig. 4A-D illustrate the obtained XPS spectra of Mn 2p, Ce 3d, O 1s and C 1s, respectively, and the corresponding surface atomic concentration and the relative concentration ratio of different oxidation state are summarized in Table 2. As shown in Fig. 4A, the Mn $2p_{3/2}$ spectra can be divided into three characteristic peaks attributed to Mn^{2+} (641.49 eV), Mn^{3+} (642.81 eV), and Mn^{4+} (644.7 eV), respectively, through peak-fitting deconvolutions.[38, 39] Mn $2p_{1/2}$ spectra showed one peak at 653.88 eV (Mn^{4+}).[31] It can be seen that the molar concentration of manganese species on the surface of MnOx-CeO_2/GR (0.3%) was lower than that of MnOx-CeO_2, which indicated that the surrounding elementary composition of manganese species could be changed by addition of GR. Furthermore, the relative surface content of manganese oxides with different valences was also changed, which played an important role in improving the electron transfer and low-temperature SCR activity of MnOx-CeO_2/GR catalysts. It was noted that the relative surface content of Mn^{4+} (Mn^{4+}/Mn) over MnOx-CeO_2/GR (58.15%) was much higher than that of MnOx-CeO_2 (49.91%). It was clear that much more Mn^{4+}/Mn species were exposed on the surface of MnOx-CeO_2/GR (0.3%), while the Mn^{4+} species and their redox cycle might be beneficial for the high activity in the NH_3-SCR reaction at low temperature, attributed to the enhancement of NO reduction to N_2.[39-42]

The Ce 3B XPS spectra are presented in Fig. 4b.The XPS spectra reveled that Ce 3d orbit was composed of two multiplets (v and u). The peaks labeled u and v were due to $3d_{3/2}$ and $3d_{5/2}$ spin-orbit states, respectively. The u, u'', and u''' and v, v'', and v''' peaks were attributed to Ce^{4+} species, while u'and v' were assigned to Ce^{3+} species.[37] No obvious difference was observed from the Ce 3d XPS spectra for MnOx-CeO_2 and MnOx-CeO_2/GR (0.3%) samples, while table 2 results implied that much more Ce species existed on the surface of MnOx-CeO_2/GR (0.3%) catalyst.

The XPS patterns of O 1s (Fig. 4C) show the presence of two types of surface oxygen in the samples. The peak at 529.4-529.7 eV corresponds to lattice oxygen (O_β), while that at 531.6-532.0eV assigned to chemisorbed oxygen (O_α, surface-adsorbed oxygen), such as O^{2-}or O^-, in the form of OH^-, and CO_3.[2-43] According to the XPS analysis, the surface concentration of O_α species on the MnOx-CeO_2/GR was higher than that of MnOx-CeO_2. It had been demonstrated that O_α species were more active than O_β species, attributing to their higher mobility.[44] Hence, the higher concentration of O_α species were beneficial to the NH_3-SCR of NO, resulting in the promotion of the reduction of NO and the subsequent facilitation of the "fast SCR" reaction.[15]

Fig. 4D shows deconvolution of the C 1s peaks in MnOx-CeO_2/GR (0.3%). A main peak at 284.1-284.6 eV was attributed to the graphitic structure,[45] and the peaks centered at about 285.9 and 288.7 eV correspond to the C-O, O-C=O, respectively.[46, 47] The existence of oxygen-containing carbon in GR shows that GR could provide active sites for directed connection with MnOx-CeO_2 particles.[30]

3.5. Redox properties

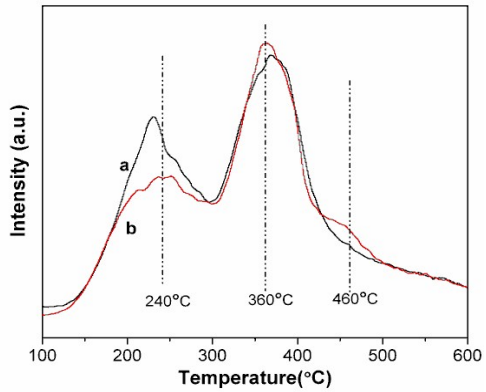

Fig. 5 H_2-TPR profiles of the catalysts: (a) MnOx-CeO_2 and (b) MnOx-CeO_2/GR (0.3%).

It is well-known that the redox property of catalysts is remarkably related to the catalytic cycle in NH_3-SCR of NO.[48] The H_2-TPR measurements are applied to evaluate the reducibility of the catalysts, and the obtained H_2-TPR profiles are illustrated in Fig. 5. For MnOx-CeO_2, the H_2-TPR profile presents two well-defined reduction peaks around 240, and 360°C, respectively. The first reduction peak represented the reduction of Mn_2O_3 to Mn_3O_4, and the second reduction peak referred to the further reduction of Mn_3O_4 to MnO and the surface reduction of CeO_2.[49-51] MnOx-CeO_2/GR (0.3%) had three reduction peaks around 240, 360, and 460°C, respectively. The intensity of the first reduction peak at about 240°C evidently decreased compared with MnOx-CeO_2, due to the molar concentration of manganese species on the surface of MnOx-CeO_2/GR (0.3%) lower than that of MnOx-CeO_2. It can be speculated that MnOx-CeO_2 had higher activity than MnOx-CeO_2/GR (0.3%) over a period of lower temperature area. The second reduction peak was higher than that of MnOx-CeO_2 sample, attributing to the fact that the content of Ce increased after the introduction of GR. Therefore, there was more surface oxygen originated from CeO_2. The third peak centered at 460°C was assigned to the reduction of surface capping oxygen of CeO_2, indicating that the mobility of oxygen species increased after the addition of GR.[52] Thus, it was reasonable to deduced that there was interaction between manganese oxide and cerium oxide species in MnOx-CeO_2/GR (0.3%), which displayed a synergistic effect in the reducibility of the catalysts, leading to the enhancement of catalytic activity.

3.6 Acidic properties

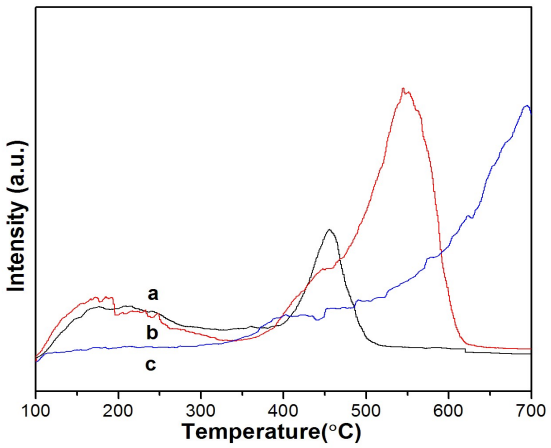

Fig. 6 NH_3-TPD profiles of the catalysts: (a) MnOx-CeO_2, (b) MnOx-CeO_2/GR (0.3%) and (c) GR.

The NH_3-TPD is performed to investigate the surface acid amount and strength of the catalysts, and the obtained NH_3-TPD profiles are shown in Fig. 6. One broad peak spanned in the temperature range of 100-300 °C was observed for both samples, attributed to NH_3 desorbed by weak and medium acid sites. For MnOx-CeO_2, desorption peaks centered at 456 °C could be associated with coordinated NH_3 molecular originating from the Lewis acid sites.[53] It can be seen that GR have not desorption peaks below 600 °C, so the desorption peaks of MnOx-CeO_2/GR (0.3%) around 550 °C could be attributed to the Lewis acid sites. The Lewis acid desorption peaks of MnOx-CeO_2/GR (0.3%) obviously shift to the high-temperature region, which suggests that the intensity of the Lewis acid sites on MnOx-CeO_2/GR (0.3%) was stronger than that of MnOx-CeO_2. In addition, it was considered that the peak area is correlated with the acid amount.[48] The NH_3-TPD profile of MnOx-CeO_2/GR (0.3%) reveals the larger peak area, especially at the high-temperature region, indicating the presence of abundant Lewis acid sites. Therefore, MnOx-CeO_2/GR (0.3%) had the stronger acid intensity due to the addition of GR, which reinforced the interaction between manganese oxide and cerium oxide species. The difference in the strength and the number of acid sites on the two catalysts might lead to the distinction of the catalytic performance.

3.7 Catalytic activity

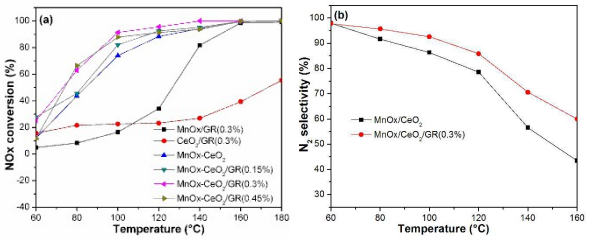

Fig. 7 (a) NH_3-SCR performance of the catalysts. (b) N_2 selectivity over the MnOx-CeO_2 and MnOx-CeO_2/GR (0.3%) catalysts. Reaction conditions: 500 ppm NO, 500 ppm NH_3, 5%O_2, and balance N_2, GHSV = 24,000h^{-1}

The activity of the prepared catalysts with the variation of temperature is presented in Fig. 7a. It can be seen that the NO conversion over all the catalysts increased with increasing temperature. The catalytic activity was enhanced with the increasing mass ratio of GR, and the MnOx-CeO_2/GR(0.3 wt.%) exhibited the highest activity. Over 100% of NO conversion was obtained at 160°C. However, the activity decreased when the mass ratio of GR rose to 0.45%. This phenomenon may be attributed to the excess graphene caused agglomeration which blocked some mesopores, resulting in the slightly decreased surface areas. It also can be acquired that the MnOx-CeO_2/GR samples had higher SCR activity compared to that of pure MnOx/GR and CeO_2/GR at low temperature region. This demonstrated that GR improved the interaction of manganese and cerium oxide species, which possibly provided more effective contact with the reactants result in oxidative sorption of NO as nitrates. N_2 product selectivity over all the catalysts as a function of temperature is shown in Fig. 7b. The N_2 selectivity of MnOx-CeO_2 and MnOx-CeO_2/GR (0.3%) catalyst was noticeably decreased above 120°C, probably attributing to the formation of N_2O at elevated temperatures. However, it reached its highest value, nearly 85%, over MnOx-CeO_2/GR (0.3%) below 120°C. Therefore, it could be concluded that MnOx-CeO_2/GR (0.3%) is very active and selective for the low-temperature NH_3-SCR of NOx.

3.8 Influence of H_2O and SO_2

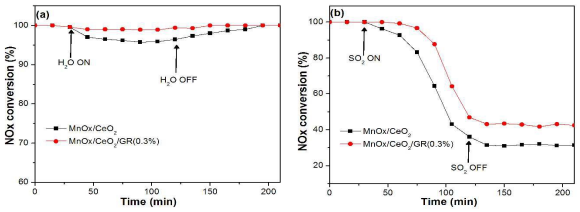

Fig. 8 (a) H_2O tolerance, (b) SO_2 tolerance of the catalysts at 180 °C. Reaction conditions: 500 ppm NO, 500 ppm NH_3, 5%O_2, 200 ppm SO_2, balance N_2, and GHSV = 24,000h^{-1}.

The H_2O and SO_2 in exhaust fumes can induce the deactivation and poisoning of catalysts.[53] Therefore, the effect of H_2O and SO_2 on NOx conversion by the MnOx-CeO_2 and MnOx-CeO_2/GR (0.3%) at 180°C were investigated. Fig. 8a shows that when 10 vol. % H_2O were added to the system, NOx conversion of MnOx-CeO_2 slightly decreased from 99% to 95%. After 1.5 h, when H_2O is removed from the flue gas, NOx conversion nearly completely recovered to original levels. This result indicated that the decrease in activity brought about by H_2O might be caused by its competive adsorption with the reactant on the active sites over the catalyst surface. However, the NOx conversion of MnOx-CeO_2/GR (0.3%) was invariant with the adding H_2O. This result indicated that the hydrophobic groups of GR are not conducive to H_2O adsorption.

The resistances of the catalysts to SO_2 poisoning were examined by feeding 200 ppm of SO_2. As illustrated in Fig. 8b, the NOx conversion of MnOx-CeO_2 decreased from the initial 100% to 36% in 1.5 h. When SO_2 feeding was switched off, catalyst activity further declined, and reached a stable level about 31%. For MnOx-CeO_2/GR (0.3%), the similar phenomenon was observed. The NO conversion decreased to 47% in 1.5 h and finally reached a stable level about 42%. These indicated that the NOx conversion of MnOx-CeO_2/GR obviously decreased but still kept relatively high activity compared with the graphene-free sample. Some ammonium sulfates can be formed by the reaction between SO_2 and the reactants (NH_3 and O_2), and the formed sulfates can occupy active sites on the surface of catalyst, deactivating the catalyst gradually. On the other hand, in combination with the XPS analysis, the content of Ce increased after the introduction of GR. It's well known that cerium oxide can act as SO_2 trap for NOx storage catalysts to limit sulfation of the main active phase when exposed to SO_2.[54] Cerium oxide inhibited the formation of manganese sulfate on the catalyst surface, hence, MnOx-CeO_2/GR convey good resistance to SO_2 in the low-temperature SCR reaction.

3.9 Stability test of the MnOx-CeO_2/GR (0.3%) catalyst and the FT-IR spectra of the fresh and poisoned MnOx-CeO_2/GR (0.3%)

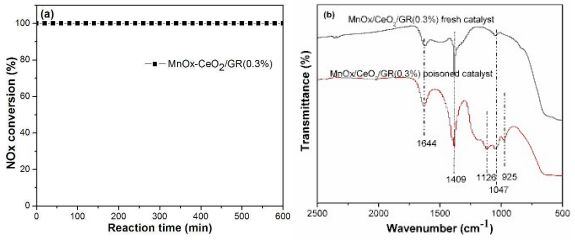

Fig. 9 (a) Stability test of the MnOx-CeO_2/GR (0.3%) catalyst. Reaction conditions: 500 ppm NO, 500 ppm NH_3, 5%O_2, 200 ppm SO_2, balance N_2, and GHSV = 24,000h^{-1}. (b) FT-IR spectra of fresh and poisoned MnOx-CeO_2/GR (0.3%) catalyst.

Stability of the MnOx-CeO_2/GR (0.3%) catalyst at 180°C is shown in Fig. 9a. The NOx conversion reached a stable level of about 100% and could last for more than 600 min. Therefore, MnOx-CeO_2/GR (0.3%) catalyst presented good stability and high SCR activity. The FT-IR spectra of the fresh and poisoned MnOx-CeO_2/GR (0.3%) are shown in Fig. 9b. Compared to the fresh catalysts, the band intensity at 1409 cm^{-1} of the poisoned catalyst was larger, due to NH^{4+} species on Lewis acid sites originated from ammonium sulfates. The peak of the poisoned sample at 1126 cm^{-1} could be attributed to the characteristic band of SO_4^{2-}, which is not observable in the fresh sample. Therefore, the introduction of SO_2 leading to the formation of byproducts such as $(NH_4)_2SO_3$ and NH_4HSO_4. The formed sulfates can occupy active sites on the surface of catalyst, deactivating the catalyst gradually.

4. Conclusion

In summary, a series of mesopores MnOx-CeO_2/graphene nanocomposites were successfully prepared by hydrothermal process. The obtained products displayed enhanced NH_3-SCR activity, higher stability, improved H_2O and SO_2 tolerance compared with MnOx-CeO_2. When GR content reached 0.3 wt %, MnOx-CeO_2/GR exhibited the best SCR catalytic performance, up to 100% at 140°C. The introduction of GR could be associated with the high specific surface areas, the uniform distribution of active sites, as well as the interaction of manganese and cerium oxide species, thus leading to the excellent catalytic performance of MnOx-CeO_2/GR. High specific surface areas provide more active sites to adsorb and activate reagents, resulting in the catalytic activity. The uniform distribution and the interaction of manganese and cerium oxide species lowered the probability of surface active sites being taken by SO_2, and decreased the formation of byproducts such as $(NH_4)_2SO_3$ and NH_4HSO_4, resulting in high catalytic cycle stability and improved SO_2 tolerance. The hydrophobic groups on the surface of GR are not conducive to H_2O adsorption. Thus the NOx conversion of MnOx-CeO_2/GR (0.3%) didn't change significantly with the adding of H_2O.

Acknowledgement

The project is financially supported by the Natural Science Foundation of Jiangsu Province (no. BK20130907), Program of Natural Science Research of Jiangsu Higher Education Institutions of China (no. 13KJB610012), the Research Startup Funds Program for High Level Talent of Nanjing Normal University (no. 2013105XGQ0056).

Reference

1 Z. M. Liu and S. I. Woo, Catal. Rev.: Sci. Eng., 2006, 48, 43-89.
2 C. H. Kim, G. S. Qi, K. Dahlberg and W. Li, Science, 2010, 327, 1624-1627.
3 J. E. Parks, Science, 2010, 327, 1584-1585.
4 Z. M. Liu, Y. Yi, S. X. Zhang, T. L. Zhu, J. Z. Zhu and J.G. Wang, Catal.Today, 2013, 216, 76-81.
5 R.B. Jin, Y. Liu, Z. B. Wu, H. Q. Wang and T. T. Gu, Chemosphere, 2010, 78, 1160-1166.
6 Z. G Huang, Z. P. Zhu, Z.Y. Liu and Q.Y. Liu, J. Catal., 2003, 214, 213-219.
7 M. Stanciulescu, G. Caravaggio, A. Dobri, J. Moir, R. Burich, J. P. Charland and P. Bulsink, Appl. Catal. B: Environ., 2012, 123-124, 229-240.
8 Y. J. Kim, H. J. Kwon, I. Heo, I. S. Nam, B. K. Choa, J. W. Choung, M. S. Cha and G. K. Yeo, Appl. Catal. B: Environ., 2012, 126, 9-21.
9 Z. Y. Sheng, Y. F. Hu, J. M. Xue, X. M. Wang and W. P. Liao, Environ. Technol., 2012, 33, 2421-2428.
10 M. Kang, E. D. Park, J. M. Kim and J. E. Yie, Appl. Catal. A: Gen., 2001, 327, 261-269.
11 S. j. Yang, C. Z. Wang, J. H. Li, N. G. Ya, L. Ma and H. Z. Chang, Appl. Catal. B: Environ., 2011, 110, 71-80.
12 B. Thirupathi and P. G. Smirniotis, J. Catal., 2012,288, 74-83.
13 G. S. Qi and R. T. Yang, Chem. Commun., 2003, 7, 848-849.
14 G. S. Qi, R. T. Yang and R. Chang, Appl. Catal. B: Environ., 2004, 51, 93-106.
15 W. P. Shan, F. D. Liu, H. He, X. Y. Shi and C. B. Zhang, Chem. Commun., 2011, 47, 8046-8048.
16 Z. M. Liu, J. Z. Zhu, J. H. Li, L. L. Ma and S. I. Woo, Appl. Mater. Interfaces, 2014, 6, 14500-14508.
17 G. S. Qi and R.T. Yang, Appl. Catal. B: Environ., 2003, 44, 217-225.
18 J. H. Huang, Z. Q. Tong, Y. Huang and J. F. Zhang, Appl. Catal., B: Environ., 2008, 78, 309-314.
19 H. Z. Chang, J. H. Li, X. Y. Chen , L. Ma, S. J. Yang, J. W. Schwank and J. M. Hao, Catal. Commun., 2012, 27, 54-57.
20 B.X. Shen, T. Liu , N. Zhao, X.Y. Yan and L. D. Deng, J. Environ. Sci., 2010, 22, 1447-1454.
21 J. Yu, F. Guo, Y. L. Wang, J. H. Zhu, Y. Y. Liu, F. B. Su, S. Q. Gao and G. W. Xu, Appl. Catal. B: Environ., 2010, 95, 160-168.
22 C. X. Liu, L. Chen, J. H. Li, L. Ma, H. Arandiyan, Y. Du, J. Y. Xu and J. J. Hao, Environ. Sci. Technol., 012, 46, 6182-6189.
23 M. oshikawa, A. asutake and I.Mochida, Appl. Catal. A: Gen., 1998, 173, 239-245.
24 X. L. Tang, J. M. Hao, H. H. Yi and J. H. Li, Catal. Today, 2007, 126, 406-411.
25 B. K. Pradhan and N. K. Sandle, Carbon, 1999, 37, 1323-1332.
26 T. V. Solís, G. Marbá n and A. B. Fuertes, Appl. Catal. B: Environ., 2003, 46, 261-271.
27 A. A. Farghali, M. Bahgat, W. M. A. El Rouby and M. H. Khedr, J. Alloys Comp., 2013, 555,193-200.
28 X. P. Pu, D. F. Zhang, Y. Y. Gao, X. Shao, G. Q. Ding, S. S. Li and S. P. Zhao, J. Alloys Comp., 2013, 55, 382-388.
29 D. H. Long, W. Li, L. C. Ling, J. Miyawaki, I. Mochida and S. H. Yoon, Langmuir, 2010, 26, 16096-16102.
30 X. N. Lu, C.Y. Song, C. C. Chang, Y. X. Teng, Z. S. Tong and X. L. Tang, Ind. Eng. Chem. Res., 2014, 53, 11601-11610.
31 X. N. Lu, C. Y. Song, S. H. Jia, Z. S. Tong, X. L. Tang and Y. X. Teng, Chem. Eng. J., 2015, 260, 776-784.
32 G. Qi, R. T. Yang and R. Chang, Appl. Catal. B: Environ., 2004, 51, 93-106.
33 Z. B. Wu, R. B. Jin, H. Q. Wang and Y. Liu, Catal. Commun., 2009, 10, 935-939.
34 B. Q. Jiang, Y. Liu and Z. B. Wu, J. Hazard. Mater., 2009,162, 1249-1254.
35 V. Subramanian, H. W. Zhu, R. Vajtai, P. M. Ajayan and B. Q. We, J. Phys. Chem. B, 2005, 109, 20207-20214.
36 M. Machida, D. Kurogi and T. Kijima, Chem. Mater., 2000, 12, 3158-3164.
37 M. Machida, D. Kurogi and T. Kijima, Chem. Mater. 2000, 12, 3165-3170.
38 D. S. Zhang, L. Zhang, L. Y. Shi, C. Fang, H. R. Li, R. H. Gao, L. Huang and J. P. Zhang, Nanoscale, 2013, 5, 1127-1136.

39 Z. H. Chen, Q. Yang, H. Li, X. H. Li, L. F. Wang and S. C. Tsang, J. Catal., 2010, 276, 56-65.
40 C. Fang, D. S. Zhang, S. X. Cai, L. Zhang, L. Huang, H. R. Li, P. Maitarad, L. Y. Shi, R. H. Gao and J. P. Zhang, Nanoscale, 2013, 5, 9199-9207.
41 B. Thirupathi and P. G. Smirniotis, J. Catal., 2012, 288, 74-83.
42 F. D. Liu, H. He, Y. Ding and C. B. Zhang, Appl. Catal., B: Environ., 2009, 93, 194-204.
43 S. Ponce, M.A. Peña and J. L. G. Fierro, Appl. Catal., B: Environ., 2000,24, 193-205.
44 F. D. Liu and H. He, J. Phys. Chem. C, 2010, 114, 16929-16936.
45 T. W. Odedairo, J. Ma, Y. Gu, J. L. Chen, X. S. Zhao and Z. H. Zhu, J. Mater. Chem. A, 2014, 2, 1418-1428.
46 G. Beamson and D.Briggs, Wiley, Chichester, 1992.
47 J. Y. Lee, S. H. Hong, S. P. Cho, S. C. Hong, Appl. Phys., 2006, 6, 996-1001.
48 L. Zhang, L.Y. Shi, L. Huang, J. P. Zhang, R. H. Gao and D. S. Zhang, ACS Catal., 2014, 4, 1753-1763.
49 X. F. Tang, Y. G. Li, X. M. Huang, Y. D. Xu, H. Q. Zhu, J. G. Wang and W. J. Shen, Appl. Catal., B: Environ., 2006, 62, 265-273.
50 W. Tian, H. S. Yang, X. Y. Fan and X. B. Zhang, J. Hazard. Mater., 2011, 188, 105-109.
51 H. F. Li, G. Z. Lu, Q. G. Dai, Y. Q. Wang, Y. Guo and Y. L. Guo, Appl. Catal., B: Environ., 2011,102, 475-483.
52 P. Concepcion, A. Corma, J. Silvestre-Albero, V. Franco and J. Y. Chane-Ching, J. Am. Chem. Soc., 2004, 126, 5523-5532.
53 K. Skalska, J. S. Miller and S. Ledakowicz, Sci. Total Environ., 2010, 408, 3976-3989.
54 R. B. Jin, Y. Liu, Y. Wang, W. L. Cen, Z. B. Wu, H. Q. Wang and X. L. Weng, Appl. Catal., B: Environ., 2014, 148-149, 582-588.

MnOx-CeO_2/graphene catalysts prepared by the hydrothermal method exhibited excellent NH_3-SCR activity and strong resistance against SO_2, which is very competitive for the practical application in controlling the NOx emission from flue gas.